INFRARED SPECTROSCOPY OF WEAKLY BOUND COMPLEXES IN SUPERFLUID HELIUM NANODROPLETS

by

EMMANUEL I. OBI, JR.

(Under the Direction of Gary E. Douberly)

ABSTRACT

The OH$\cdots$CH$_4$ complex has been isolated in superfluid helium nanodroplet matrices. The infrared spectrum in the region of the OH stretch ($\sim$3562 cm^{-1}) has been collected. What should be single transitions as compared to the spectrum for the OH radical in superfluid helium are split into triplets. The origin of this splitting pattern is thought to be the K states of the internal rotor projected onto the intermolecular axis. Systematic deuteration allowed for the collection of three other isotoplogue specta: $OD\cdots CH_4$, $OH\cdots CD_4$, and $OD\cdots CD_4$. Splitting of lines belonging to the heaviest isotopologue are virtually non-existent. This provides an interesting opportunity to study the effects controlling the moment of inertia of a weakly bound complex can have on its ability to exhibit large amplitude motions. Current progress and a framework for future consideration is presented.

INDEX WORDS: spectroscopy, van der Waals complex, weakly bound complex, angular momentum, angular momentum coupling, matrix isolation

INFRARED SPECTROSCOPY OF WEAKLY BOUND COMPLEXES IN SUPERFLUID HELIUM NANODROPLETS

by

EMMANUEL I. OBI, JR.

B.S. Chem., University of Georgia, 2011

A Thesis Submitted to the Graduate Faculty
of The University of Georgia in Partial Fulfillment
of the
Requirements for the Degree

MASTERS OF SCIENCE

ATHENS, GEORGIA

2014

INFRARED SPECTROSCOPY OF WEAKLY BOUND COMPLEXES IN SUPERFLUID HELIUM NANODROPLETS

by

EMMANUEL I. OBI, JR.

Approved:

Major Professor:	Gary E. Douberly
Committee:	Michael A. Duncan Geoffrey D. Smith

Electronic Version Approved:

Julie Coffield
Interim Dean of the Graduate School
The University of Georgia
August 2014

Spectroscopy of Weakly Bound Complexes in Superfluid Helium Nanodroplets

Emmanuel I. Obi, Jr.

July 28, 2014

Acknowledgments

For my fiancé, Kristin, who throughout this process supported me not just with love and understanding, but with a tolerance for the arcane that I'd like to think led to the perfection of her chocolate-chp cookie recipe.

Contents

List of Figures

List of Tables

Chapter 1

Introduction

1.1 One species of atmospheric relevance: the OH-CH_4 complex

Kirschke and co-workers [1], report that the mole fraction of CH_4 in the atmosphere has steadily risen since the 1980s while there has been a general decline (with significant fluctuation) in its yearly growth rate. In recent times (since 2006) however, there has been growth in the atmospheric mole fraction of methane and lapse in the growth rate. That is, less CH_4 is being released into the atmosphere every year while its relative abundance continues to grow. It is thought that the liberation of natural gas through the expansion of the hydraulic fracturing practice along with the release of methane from the warming of permafrost [1] will only continue to strain on the Earth's oxidative capacity to mitigate the greenhouse gas. This discrepancy in the growth rate of methane and the concentration suggests an imbalance between the sources and sinks for CH_4 whose origin is not well understood.

A strong kinetic isotope effect observed in kinetics experiments [2] on the reaction between CH_4 and OH suggests that the reaction proceeds via hydrogen abstraction. The work of Lester and co-workers seems to support hydrogen abstraction. They report homogeneous broadening of rovibrational overtone lines [3] belonging to OH of the complex indicate shortened lifetime of OH vibrational activation. They attribute decay of the hydroxyl radical overtone to resonant vibrational energy transfer to methane vibrational modes via an inelastic scattering pathway. It is not clear what bearing such energy partitioning has on the reactive path but understanding this phenomenon may prove relevant to the mechanisms involving vibrationally excited reactants.

Typical one-step reactions follow the Arrhenius prescription and exhibit a linear relationship between the rate constant and temperature. The log of the rate constant is plotted versus the temperature reciprocal and displays a negatively-sloping curve. This behavior is indicative of a positive activation energy barrier [4]. That is, as temperature increases, so does the reaction rate. Such a relationship is colloquially referred to as ‘Arrhenius’ behavior. Reaction between neutral molecules typically exhibits Arrhenius behavior as available internal energy of the system is used to overcome an activation barrier owing to steric hindrance between the reactants.

Reactions exhibiting non-Arrhenius behavior, are said to have ‘negative’ activation energies. Deviations from Arrhenius behavior present as non-linear Arrhenius plots. The simplest deviation is absence of an activation barrier. Reactions such as these are referred to as ‘barrierless’ processes. Increasing the available reaction energy has the opposite effect than on traditional Arrhenius reactions and so acts to inhibit reaction progress by diminishing the number of reactant pairs in the appropriate orientation for reaction. Lower reaction temperatures increase the likelihood that long-range interactions (van der Waals forces) ensure approaching reactants are guided to the appropriate orientation. Such reaction behavior is the origin of negative temperature dependence [5]. Arrhenius plots for such processes exhibit monotonic increase and saturation in the log of the rate constant as environment temperature is reduced. Radical-radical association reactions are perfect examples that show this type of non-Arrhenius behavior. Spectroscopic study of association products of such reactions has been the recent focus of experiments conducted by the Douberly group.

The more complicated type of non-Arrhenius behavior are exhibited by those reactions that have an entrance channel complex. As reactants approach along the reaction path, they are guided towards a van der Waals minimum (whose manifestation is usually barrierless) by long-range interactions. The temperature-dependent evolution of the rate constant for these reactions display characteristics of both 'barriered' and barrierless reactions. At sufficiently high temperatures (where $kT < D_0$), the reaction progress bypasses the weakly-bound intermediate altogether leading to the linear Arrhenius behavior indicative of a one-step reaction. The complication is introduced at temperatures lower than the dissociation energy of the complex. At such temperatures, reaction progress from these weakly-bound states essentially introduces two competing steps to the reaction mechanism as the reactants can redissociate or proceed over some 'inner' barrier [6]. As temperature is decreased further, deviation of the overall rate constant from Arrhenius behavior becomes more apparent leading ultimately to a minimum in the rate constant. Relative to the energy of separated reactants, the inner barrier can be submerged. Atkinson shows, in an Arrhenius plot of CH_4 + OH reaction rates measured at various temperatures ($\sim$250-2000 K) collated from various experiments [2], that the reaction rate very closely follows typical Arrhenius behavior. Slight curvature of the featured Arrhenius plot is accounted for by including a near-cubic (2.82) temperature dependence in the pre-exponential factor of the fitting equation. This suggests the presence of a weakly bound complex.

Low-temperature spectroscopic studies of the OH-CH_4 complex will serve to guide development of accurate potential energy surfaces for prediction of atmospheric concentrations.

1.2 Rigid vs. non-rigid molecules

Molecular spectroscopists endeavor to probe the bound states of groups of atoms. The molecule is an equilibrium configuration of this atom group capable of absorbing only discrete quantities of electromagnetic radiation. The discrete absorptions of radiation occur because some motion (or, more interestingly, a convolution of motions) of atoms within the molecule are in resonance with the frequency of absorbed radiation. Atomic motion is dynamical and so naturally described by an eigenfunction of a differential operator. The differential operator—the Hamiltonian—is a version of the wave equation and so its eigenfunctions are called *wavefunctions*. Unlike describing classical phenomena, wavefunctions associated with the motions of molecules are quantum in nature. Indeterminacy in measuring conjugate variables such as the position and velocity (or, more pertinent to the work of a spectroscopist, the variables time and energy) of atoms in a molecule leads to a strange, statistical interpretation of the wavefunction whose modulus is interpreted as a likelihood of the molecule exhibiting some behavior [7]. Not unlike boundary conditions placed on a vibrating string [8], it is the potential energy born from interatomic forces that serves to bind the wavefunction of a molecule. These bound states are visualized as wells on a potential energy map with respect to one or more degrees of freedom. Detected resonances are traditionally fashioned to appear as intensity peaks over a spectrum of frequencies. These resonances typically correspond to angström-sized displacements from equilibrium. These are the *small amplitude motions* and are indicative of a quantum state bound by a relatively 'deep' well on the potential energy surface. The small amplitude motion is associated with strongly bound molecules and is the stuff of popular pedagogy in spectroscopy [9, 10].

As discussed in a recent editorial [11], it is near the dissociation limit or when the binding potential is shallow that "real" chemistry is happening. Near the binding threshold of a potential energy well, there is a high density of states which leads to significant mixing of bound state wavefunctions. In the case of a shallow well, tunneling out of the bound state can also lead to significant state mixing. Both scenarios outline situations where molecular motions venture far[1] from equilibrium. This is the realm of *large amplitude motions.* The spectra of molecules exhibiting this behavior are not always clear and present a current challenge in the field of spectroscopy.

Another example of large amplitude motion is contortion. Molecules of high symmetry tend to have identical nuclei. Atoms are considered identical if they can be traded across a mirror plane without consequence to the overall configuration of the molecule. Such permutation of identical nuclei is said to leave the molecule in a configuration indistinguishable from its original since the Hamiltonian is invariant to permutation of identical nuclei [12]. Transformations between indistinguishable molecular configurations are facilitated by complete; nuclear; permutation; inversion (CNPI) group operations [12, 13]. Examples of such transformations include the fluxional inversions of both the nitrogen atom of ammonia [14] or the acetylenic hydrogen in the vinyl radical [15, 16]. These motions are referred to as contortions and are characteristic of what are known as non-rigid molecules. Non-rigid molecules are called such because they sample indistinguishable stationary states through some contortion mode. Typically, there exists a barrier along the contortion coordinate. If the well depth is sufficient and the internal energy of the molecule is low enough for occupation of a bound state in the double-well potential (figure 1.1), tunneling splittings can be observable in the spectrum. Energy level separations between bound contortion states depend on the height and width of the barrier and also on the mass of the atom(s) undergoing along the contortion path [7].

Molecules that undergo large amplitude motions sample wider swathes of the potential energy surface. The presence of this behavior can then be used as an indicator of the rigidity of the molecule. Simply put, *rigid molecules* are those that only exhibit small amplitude

---

[1] On the order of the equilibrium bond length or angle [12]

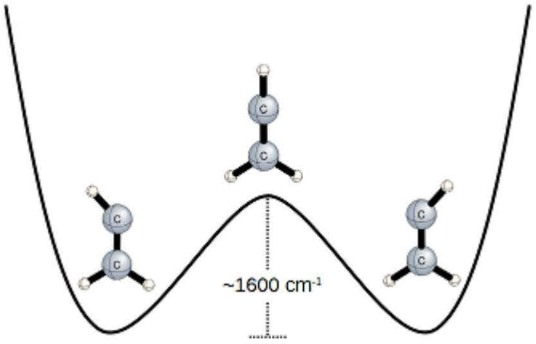

Figure 1.1: Cartoon of a "W" potential along the contortion coordinate of vinyl radical, acetylenic hydrogen tunneling.

motions. A *non-rigid molecule* has at least one large amplitude motion coordinate. The presence of such a coordinate distorts the symmetry of the equilibrium configuration and can allow transition intensity where before there was none. Molecules bound by van der Waals forces present an ideal class of systems for studying the presence of these types of motions. The translational degrees of freedom of monomers bound in the formation of a complex are transformed into large amplitude bending vibrations. This is especially the case for analyzing the bending modes of atom-diatom systems [17–20]. In systems where the atom is replaced by a molecule, this large amplitude bending becomes an internal rotation. Internal rotation in weakly bound complex is the focus of this thesis.

1.3 The importance of coordinate systems

A wavefunction that describes all possible behavior of the molecule—electronic, vibrational, rotational, and translational—can be unwieldy to write analytically [21] especially when dealing with molecules having more than two atoms. This makes simplification of such a wavefunction a priority. Being a differential operator, the Hamiltonian naturally has exponential eigenfunctions parametrized by appropriate quantum numbers. Such functions lend themselves well to the separation of variables. In the collection of high-resolution spectra, regardless of the energy regime, an understanding of a perturbation (i.e. internal rotation) that causes distortion of the zeroth order picture is elusive without a foundational grasp of the coordinates which best simplify the wavefunction. An overview of such a foundation is covered here.

The crudest coordinate frame for the description of molecular behavior is that of the space-fixed, XYZ axes. In this frame, no degrees of freedom are separablethat is, as the molecule moves through space, there is linear momentum imparted on the molecular center of mass. This means that the total energy of the molecule depends on the speed at which it moves. Such a formulation is not generally helpful to molecular spectroscopy concerned primarily with the internal states of a molecule [12]. A more useful formulation is the use of a coordinate frame whose origin is located at the molecular center of mass. This allows for the separation of the translational wavefunction from that of the internal wavefunction. That is, as the molecule moves through space, coordinates describing electronic and nuclear displacement vectors remain constant. It is the XYZ axes that improve on the use of the XYZ axes and form a basis for the space-fixed, molecular center of mass coordinates. Focus can now be directed towards the internal wavefunction concerned with only the electronic, vibrational, and rotational degrees of freedom.

Although confined to the spectral window to which one can afford, the measuring of spectra is the easy part. It is deriving meaning from the spectrum that can be tricky. This problem is compounded for those using light sources of narrow linewidths (on the order of 1 MHz—0.03 cm^{-1}) as the structure of convolved states can be revealed. Describing the levels probed by an experiment can be made less difficult though variable separation of the wavefunction. Since the eigenfunctions of the internal Hamiltonian are some form of exponential function, its factoring into a product of functions for each degree of freedom creates an efficiency. Eigenvalues of such a factored Hamiltonian are a sum of eigenvalues.

Instead of fixing the origin of the coordinate system at the molecular center of mass as in the XYZ reference frame, the origin can be placed at the nuclear center of mass. Such a placement allows for the separation of the electronic from the nuclear degrees of freedom (otherwise known as the Born-Oppenheimer approximation). That is to say that as the electrons are displaced, the center of mass is not. This allows for separate descriptions of the electronic wavefunction and the rovibrational wavefunction as the new coordinate frame is said to have a basis in the $\xi\eta\zeta$ axes which is the nuclear, space-fixed reference frame. Proper separation of the rovibrational wavefunction is the problem of accurately assigning resonances of high-resolution infrared spectroscopy.

In the $\xi\eta\zeta$ space-fixed frame of reference, a change in the orientation of a given nuclear configuration also changes the vectors that describe nuclear displacement. Rotation and vibration are convolved. The rovibrational wavefunction can be separated into a rotation and a vibration wavefunction by definition of the Euler angles $\phi, \theta, and \chi$. The Euler angles parametrize rotations within a given frame of reference [12, 22–24]. That is, the Euler angles provide a mapping from the coordinates of a given function to its rotated analogue. Such a mapping is achieved through rotation of xyz axes that begin as superimposed on the $\xi\eta\zeta$ axes.[2] The orientation of the molecule is fixed in the xyz frame of reference and it is the xyz axes that are transformed by successive application of rotation operators through the Euler angles[3] as shown in figure 1.2 below. This molecule-fixed frame[4] is transformed first by counter-clockwise rotation of the xy/$\xi\eta$ plane about the *figure*, ζ, axis through the azimuthal angle, ϕ. The next rotation separates the superimposed $\xi\eta$ and xy planes by clockwise rotation about an axis that lies mutually perpendicular to the ζ and z axes

---

[2] If Euler angles are defined relative to the XYZ coordinate axes, they are generally referred to as $\alpha, \beta,$ andγ rather than $\phi, \theta,$ andχ which are reserved for the xyz frame.

[3] Rotation in this fashion is considered 'passive'. This is contrary to the intuitive 'active' rotation that directly transforms vector coordinates. Either the vector in a given frame is transformed to the *same vector in a new frame* or is taken to a *new vector in the same frame*. This subtle distinction is highlighted by several authors [22–25], the passive vs. active perspectives on rotational transformation are inversely related.

[4] Also referred to as the *body*-fixed frame

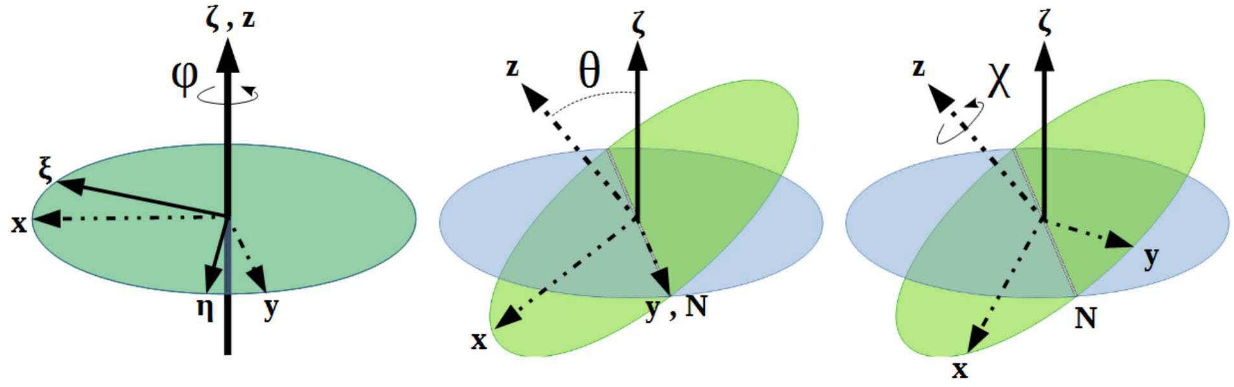

Figure 1.2: The Euler rotations that connect the $\xi\eta\zeta$ frame to the xyz frame.

through the polar angle, θ. The axis of polar rotation is known as the 'line of nodes' [22–24], N, as it represents the axis defined by the line belonging to both the xy and $\xi\eta$ planes. The last rotation is simply one counter-clockwise about the transformed z axis and defines the χ angle. These three coordinate frame rotations find analogue in the Cartesian rotation matrices. Sequential multiplication of the representative rotation matrices gives a total rotation transform that is described by the rotation matrix shown below. This matrix is the direction cosine matrix that represents the transform from space-fixed to molecule-fixed reference frames.

$$R_z(\chi) \cdot R_N(\theta) \cdot R_\zeta(\phi) = \begin{bmatrix} \cos\chi & -\sin\chi & 0 \\ \sin\chi & \cos\chi & 0 \\ 0 & 0 & 1 \end{bmatrix} \begin{bmatrix} \cos\theta & \sin\theta & 0 \\ 0 & 1 & 0 \\ sin\theta & 0 & \cos\theta \end{bmatrix} \begin{bmatrix} \cos\phi & -\sin\phi & 0 \\ \sin\phi & \cos\phi & 0 \\ 0 & 0 & 1 \end{bmatrix} \tag{1.1}$$

$$\mathbf{R} = \begin{bmatrix} \cos\theta\cos\phi\cos\chi - \sin\phi\sin\chi & \cos\theta\sin\phi\cos\chi + \cos\phi\sin\chi & -\cos\theta\sin\chi \\ -\cos\theta\cos\phi\sin\chi - \sin\phi\cos\chi & -\cos\theta\sin\phi\sin\chi + \cos\phi\cos\chi & \sin\theta\sin\chi \\ \sin\theta\cos\phi & \sin\theta\sin\phi & \cos\theta \end{bmatrix} \tag{1.2}$$

While Cartesian representations of rotation operators (i.e. the rotation matrices as shown in equation refeq:rotation1) are useful in describing vector frame transformations, they are not the operators that generate rotation of rovibrational wavefunctions. For convenience here, the spherical harmonics[5] are used as wavefunctions. In order to derive a function operator isomorphic [26] to the Cartesian rotation matrices, it is appropriate to consider the notion of an *infinitesimal operator.* As follows from Zare [24], consider a unitary operator, $\mathbf{U}$, composed of the sum between the identity, $\mathbf{I}$, and some operator, i$\delta\mathbf{S}$ (equation 1.3). In the limit of an infinitesimal δ value, the operator $\mathbf{U}$ is virtually unchanged and is essentially just the identity.

$$\mathbf{U} = \mathbf{I} + i\delta\mathbf{S} \tag{1.3}$$

Suppose $\mathbf{U}$ is applied n number of times, the $\mathbf{U}$ operator can then be written as the following

$$\mathbf{U}^n = (\mathbf{I} + i\delta\mathbf{S})^n \tag{1.4}$$

$$\lim_{n\to\infty}\left(\mathbf{I} + i\frac{\varepsilon}{n}\mathbf{S}\right) = \mathbf{I} + i\varepsilon\mathbf{S} + \frac{(i\varepsilon\mathbf{S})^2}{2!} + \frac{(i\varepsilon\mathbf{S})^3}{3!} + \cdots \tag{1.5}$$

$$= \sum_{n=1}^{\infty}\frac{(i\varepsilon\mathbf{S})^n}{n!} \tag{1.6}$$

where ε is the parameter representing the extent to which $\mathbf{S}$ has transformed the system. The expansion of equation 1.5 is the result of multiple applications of $\mathbf{U}$. This leads to the powers series expression in equation 1.6 which, in the limit of infinite n is equivalent to an exponential.

$$\lim_{n\to\infty}\left(\mathbf{I} + i\frac{\varepsilon}{n}\mathbf{S}\right) = e^{i\varepsilon\mathbf{S}} \tag{1.7}$$

The exponential operator is also unitary. In replacing $\mathbf{S}$ with the projection of the angular momentum operator, $\mathbf{J}$, onto some unit vector, $\hat{n}$, the angular momentum operator projection onto $\hat{n}$ is said to *generate rotation about* $\hat{n}$. This is owed to the form of the projected angular

---

[5] They form an orthonormal set and are well known (purely rotational) eigenfunctions of both the rovibrational Hamiltonian and the total angular momentum operator, $\mathbf{J}^2$ [12, 21]

momentum operator since it is a differential operator written as follows

$$\mathbf{J} \cdot \hat{n}_\varepsilon = \mathbf{J}_\varepsilon = -i\frac{\partial}{\partial\varepsilon}. \tag{1.8}$$

The exponential rotation operators generated by projection of the angular momentum operator onto some axis are isomorphic to the Cartesian rotation matrices and so can also be used to compose the Euler rotations. This is done in the same way as in equation 1.1.

$$\mathbf{R}_n(\varepsilon) = e^{i\varepsilon\mathbf{J}\cdot\hat{n}} = e^{-i\varepsilon\mathbf{J}_n} = e^{-i\varepsilon\frac{\partial}{\partial\varepsilon}} \tag{1.9}$$

$$\mathbf{R}(\phi, \theta, \chi) = e^{-i\chi\mathbf{J}_z}e^{-i\theta\mathbf{J}_N}e^{-i\phi\mathbf{J}_\zeta} \tag{1.10}$$

As with Cartesian rotation, the Euler rotation begins with rotation about the ζ axis, then rotation about the line of nodes, and ends with rotation about the z axis. Note that the series of rotations are not all with respect to the one coordinate frame. The product in equation 1.10 can be written with respect to the space-fixed coordinate frame [24] and is shown below

$$\mathbf{R}(\phi, \theta, \chi) = e^{-i\phi\mathbf{J}_\zeta}e^{-i\theta\mathbf{J}_\eta}e^{-i\chi\mathbf{J}_\zeta}. \tag{1.11}$$

Writing the complete Euler rotation with respect to a consistent reference frame ($\xi\eta\chi$) as in equation 1.11 requires that the the η axis be defined as coinciding with the 'line of nodes'. The rotation operator, $\mathbf{R}(\phi, \theta, \chi)$, is now be compatible with the spherical harmonics.

The principle axis[6] for a given spherical harmonic is chosen to initially be parallel with the the coincident (ζ) and z axes. In this position, the function is an eigenvalue of $\mathbf{J}^2$, $\mathbf{J}_\zeta$, and $\mathbf{J}_z$. Upon rotation of the molecule-fixed frame—application of $\mathrm{R}(\phi, \theta, \chi)$ of equation 1.11—the spherical harmonic remains an eigenfunction of $\mathbf{J}^2$ and $\mathbf{J}_z$, but is no longer an eigenfunction of $\mathbf{J}_\zeta$ as the quantization axis has been displaced [27]. The spherical harmonics then

---

[6] Also referred to as the *figure axis*

are no longer the simultaneous eigenfunctions for the three angular momentum operators considered. A more general function is needed.

In field-free space, there is energetic degeneracy of the spherical harmonics having the same order, ℓ, but different degree, m. This means the linear combination of spherical harmonics belonging to the (2ℓ+1)-dimensional, m-manifold of functions is also an eigenfunction of the Hamiltonian. Since the Hamiltonian commutes with $\mathbf{J}^2$, the m-manifold of functions also serves as a simultaneous eigenfunction for $\mathbf{J}^2$. Individual rotation operators, $\mathbf{R}_n(\varepsilon)$ of equation 1.9 that comprise $\mathbf{R}(\phi, \theta, \chi)$, can be shown to also commute with $\mathbf{J}^2$. The m-manifold can then serve as a simultaneous eigenfunction of all three operators: the Hamiltonian, $\mathbf{J}^2$, and $\mathbf{J}_\zeta$.

$$Y_{\ell m} = \sum_{n=-\ell}^{\ell} c_n Y_{\ell n}, \text{ where } c_n = 0 \text{ for } n \neq m. \tag{1.12}$$

$$\mathbf{R}(\phi, \theta, \chi) Y_{\ell m} = Y'_{\ell m} \tag{1.13}$$

$$\mathbf{R}(\phi, \theta, \chi) Y_{\ell m} = \sum_{m'=-\ell}^{\ell} c_{m'} Y_{\ell m'} = \sum_{m'=-\ell}^{\ell} Y_{\ell m'} c_{m'} \tag{1.14}$$

$$\mathbf{R}(\phi, \theta, \chi) Y_{\ell m} = \sum_{m'=-\ell}^{\ell} Y_{\ell m'} D^{\ell}_{m'm} \tag{1.15}$$

$$\text{where } D^{\ell}_{m'm} = Y^*_{\ell m'} \mathbf{R}_z(\phi) \mathbf{R}_y(\theta) \mathbf{R}_\zeta(\chi) Y_{\ell m} = Y^*_{\ell m'} \mathbf{R}(\phi, \theta, \chi) Y_{\ell m} \tag{1.16}$$

Application of $\mathbf{R}(\phi, \theta, \chi)$ can be thought of as projecting a given function $|\ell, m\rangle$ onto the (2ℓ+1)-dimensional sub-space of spherical harmonics, $Y_{\ell m}$, where the $c_{m'}$ coefficients are non-zero as shown in equation 1.14. The expansion coefficients of equation 1.14 are actually matrix elements of the well known *Wigner D-matrices* [27] defined in equation 1.16. The $\mathbf{R}_{\hat{n}}(\varepsilon)$ rotation operators that comprise $\mathbf{R}(\phi, \theta, \chi)$ can be substituted into equation 1.16 to give the following

$$D^{\ell}_{m'm} = \langle \ell m' | \left(e^{-i\phi \mathbf{J}_\zeta} e^{-i\theta \mathbf{J}_\eta} e^{-i\chi \mathbf{J}_\zeta} \right) | \ell m \rangle \tag{1.17}$$

$$D^{\ell}_{m'm} = e^{i\phi m'} \langle \ell m' | \, e^{-i\theta \mathbf{J}_\eta} \, | \ell m \rangle \, e^{-i\chi m} \tag{1.18}$$

$$D^{\ell}_{m'm} = e^{i\phi m'} d^{\ell}_{m'm}(\theta) e^{-i\chi m}, \tag{1.19}$$

The analytical forms of the 'small-d' Wigner matrices of equation 1.19 are unimportant here and given elsewhere [22, 24]. By combining equations 1.13, 1.14 and 1.16, the needed generalized spherical harmonics can be written.

$$Y'_{\ell m} = Y_{\ell m}(\phi', \theta', \chi') = \sum_{m'=-\ell}^{\ell} D^{\ell}_{m'm}(\phi, \theta, \chi) Y_{\ell m'} \tag{1.20}$$

More generally, the eigenfunctions referenced in equation 1.20, above, may be written in terms of the eigenvalues of $\mathbf{J}^2$ and $\mathbf{J}_\zeta$ like $|JM\rangle$. The Wigner D-matrices are written as $D^{J}_{M'M}$ in such a convention. Unrotated rigid-body eigenfunctions in the space-fixed frame can now be related to the rotated eigenfunctions of the molecule-fixed frame.[7]

$$|JM\rangle_R = \sum_{M'=-J}^{J} D^{J}_{M'M}(\phi, \theta, \chi) \, |JM'\rangle \tag{1.21}$$

$$|JM\rangle_R = \sum_{M'=-J}^{J} \langle JM' | \, \mathbf{R}(\phi, \theta, \chi) \, |JM\rangle \, |JM'\rangle \tag{1.22}$$

The above equation is a general form of equation 1.20 where the M' is the projection of the space-fixed angular momentum onto the rotated z axis. The use of a conjugate Wigner D-matrix, in the following equations, invokes an inverse rotation. In the following, M'' is

---

[7] Rotated kets bear the $_R$ subscript and the use of primes designates an initial orientation rotated in a rotated frame

the angular momentum projection of the rotated figure axis onto the space-fixed axis.

$$\sum_{M=-J}^{J} D^{*J}_{M''M}(\phi',\theta',\chi')\,|JM\rangle_R =$$

$$\sum_{M=-J}^{J}\sum_{M'=-J}^{J} D^{*J}_{M''M}(\phi',\theta',\chi')\,\langle JM'|\,\mathbf{R}(\phi,\theta,\chi)\,|JM\rangle\,|JM'\rangle$$

$$= \sum_{M=-J}^{J}\sum_{M'=-J}^{J} |JM''\rangle_R\,\mathbf{R}^{-1}(\phi',\theta',\chi')\,\langle JM|_R\,\langle JM'|\,\mathbf{R}(\phi,\theta,\chi)\,|JM\rangle\,|JM'\rangle$$

$$= \sum_{M=-J}^{J}\sum_{M'=-J}^{J} |JM''\rangle\cdot\langle JM|_R\,\langle JM'|\cdot|JM\rangle_R\,|JM'\rangle$$

After some rearrangement, the double sum above reduces to a single ket, $|JM''\rangle$.

$$\sum_{M=-J}^{J} D^{*J}_{M''M}(\phi',\theta',\chi')\,|JM\rangle_R = |JM''\rangle \tag{1.23}$$

$$\sum_{K=-J}^{J} D^{*J}_{MK}(\phi',\theta',\chi')\,|JK\rangle_R = |JM\rangle \tag{1.24}$$

The Wigner D-matrices, as per equation 1.16, are measures of the effect of rotation on a given rotational eigenfunction—that is, the Wigner D-matrix elements give the likelihood that a space-fixed function having angular momentum projection M will have projection K onto the figure axis in the rotated, molecule-fixed frame. Rotation operators acting on the xyz frame, $\mathbf{R}(\phi,\theta,\chi)$, form a set of transforms of all rotations about all axes passing through the nuclear center of mass form. This set is a non-abelian group known as K(mol)[8] and is a sub-group of the rotation group, SO(3) [26]. As shown in equation 1.24, the function $|JM\rangle$ is projected onto a $(2J+1)$-dimensional basis of $|JK\rangle_R$ functions. This set of basis functions is

---

[8] K(spatial) is another sub-group of SO(3). It is the set of all *space-fixed* rotations and is isomorphic to K(mol) [12]

an *irreducible representation*[9] of $|JM\rangle$ [12,24] that is referred to as $D^{(J)}$. So upon rotation, $|JM\rangle$ can be said to transform irreducibly under the set $D^{(J)}$. Each value of J has its own basis and J can take an infinite number of values. This means that there are an infinite number of irreducible representations. Since a given $|JM\rangle$ can be represented by a $D^{(J)}$ basis of arbitrary rotation,[10] the $D^{(J)}$ bases can then serve as irreducible representations of the aforementioned K(mol) group of molecule-fixed rotations.

Operators of the group SO(3) preserve vector length as well as the inner product between vectors. This means that upon rotation of a spherical harmonic, the order of the function, ℓ, remains unchanged. It is only the orientation of the function that is changed. Wavefunctions having such a property are said to be *rotationally invariant*. That is, energy and total angular momentum are conserved because the rotation operator commutes both with the Hamiltonian and the $\mathbf{J}^2$ operators, respectively. Similar to the situation of equation 1.12, there is a single dominant term in equation 1.24. This lone Wigner D-matrix can be normalized for rotation through χ [24] and as such is the sought-after general rotational eigenfunction.

$$|JKM\rangle = \left(\frac{2J+1}{8\pi^2}\right)^{1/2} D^{*J}_{MK} \tag{1.25}$$

These $|JKM\rangle$ functions are the ideal symmetric top wavefunctions because they transform as the irreducible representations of the group K(mol). This greatly simplifies the determination of transitions as evaluation of matrix elements making use of these functions must contain the dipole moment representation, $D^{(1)}$.

If wavefunctions can be rotated and projected onto an irreducible representation, then maybe the same can be done for operators. Such a maneuver would simplify the evaluation of operator matrix elements. In a general sense, a *spherical tensor operator* is one that has this property.

---

[9] Meaning the $(2J+1)$-dimensional sub-space is linearly independent

[10] Any rotation of a basis set $D^{(J)}$ still serves as a perfectly suitable representation for the function $|JM\rangle$ albeit with different coefficients

The unit vectors about which Euler rotations are generated ($\hat{n}_\varepsilon = \hat{n}_\phi, \hat{n}_\theta, \hat{n}_\chi$) will be referred to as the 'Euler vectors'. These vectors have components in the space-fixed $\xi\eta\zeta$ frame.[11] The first unit vector is $\hat{n}_\phi$ and is coincident with the space-fixed unit vector, $\hat{n}_\zeta$. The second, $\hat{n}_\theta$, is in the $\xi\eta$ plane and so can be written in terms of $\hat{n}_\xi$ and $\hat{n}_\eta$. The last unit vector, $\hat{n}_\chi$, has projections on all three axes. With the Euler vectors written with respect to the space-fixed unit vectors, the angular momentum operator, $\mathbf{J}$, can be applied. The dot product between $\mathbf{J}$ and the $\hat{n}_{\xi,\eta,\zeta}$ vectors gives the space-fixed angular momentum component operators, $\mathbf{J}\xi, \eta, \zeta$, following equation 1.8. The angular momentum component operators of the space-fixed frame can then be summed to compose a form of the total angular momentum operator that is written *in terms of the Euler angles*. By applying the direction cosine matrix (equation 1.2) to the space-fixed unit vectors, new angular momentum operators can be composed *also* in terms of the Euler angles—this time with respect to the molecule-fixed frame, xyz. The $\mathbf{J}^2$ operator is the same in either reference frame and is featured below

$$\mathbf{J}^2 = -\frac{\partial^2}{\partial\theta^2} - \cot\theta\frac{\partial}{\partial\theta} - \frac{1}{\sin^2\theta}\left(\frac{\partial^2}{\partial\phi^2} + \frac{\partial^2}{\partial\chi^2} - 2\cos\theta\frac{\partial^2}{\partial\phi\partial\chi}\right) \tag{1.26}$$

It is the angular momentum component operators that differ when written with respect to both frames. While the $\mathbf{J}\xi, \eta, \zeta$ operators with respect to the space-fixed frame have the usual commutation properties [12, 21, 24], those with respect to the molecule-fixed frame do not. The difference is illustrated by the behavior of the ladder operators, $\mathbf{J}_{+/-}$. For example, the $\mathbf{J}_+$ operator in the space-fixed frame 'raises' the value of the angular moment quantum number while those in the molecule-fixed frame 'lowers' the quantum number. The $\mathbf{J}_{x,y,z}$ of the molecule-fixed frame are said to have *anomalous commutation* properties the origin of which are discussed elsewhere [12, 13, 24].

---

[11] The space-fixed unit vectors ($\hat{n}_{\xi,\eta,\zeta}$) are those that lie along the space-fixed axes of the $\xi\eta\zeta$ frame

What is presented here is the general framework for solving hard problems in spectroscopy. Shown elsewhere [12, 22–24], the angular momentum operators and the dipole moment operators can be cast as spherical tensor operators. Doing this simplifies the work of evaluating the matrix elements of coupled systems.

1.4 The pseudo-diatomic molecule

When considering how to most precisely describe the infrared spectra of a weakly bound complex, it is necessary to include rovibrational coupling of *intra*molecular modes in each monomer as well as *inter*molecular mode coupling through the weak bond. This is tedious and usually impractical. Alternatively, the monomer orientation angles relative to the internuclear axis that connects the monomer centers of mass can be assumed averaged (over a rotational period of the complex) and their vibrational degrees of freedom frozen. These assumptions allow the monomers to be effectively treated as point masses positioned about the bimer center of mass. The simplest system to which such a simplification is applied are the prototype rare gas; diatomic molecule systems [17–19, 28]. Such an approach is known as the *pseudo-diatomic approximation.* Balle and co-workers [28] use an angle-averaged radial potential in their pseudo-diatomic treatment of Kr$\cdots$HCl. The effectiveness of their approximation owes to the accuracy with which it predicts the reduced mass of the complex [28]. Success of the model suggests that coupling between the radial and angular components of the intermolecular potential is usually small enough to be ignored [29]. Breakdown of the model can happen for complexes of reasonably large monomers as the rotation-vibration interaction constant increases commensurate with reduction in the rotational constant of the pseudo-diatom.

In continuing with the simplest pseudo-diatom, there are three elements at play governing the rotational energy level structure: the angular momentum of the diatomic monomer, the angular momentum of the entire complex, and the interaction potential that couples the internal rotor to the intermolecular axis. These three factors combine in various ways not unlike in Hund's famous coupling cases [30,31] for describing angular momentum of diatomic molecules. Parallels can be drawn between the *spinless* angular momentum vector, $\vec{N} = \vec{R} + \vec{L}$, of a diatomic molecule and the total angular momentum of a pseudo-diatom, $\vec{J} = \vec{\ell} + \vec{j}$.[12] When the interaction potential that couples angular momentum of the internal rotor to that of the complex is much smaller than the rotational energy of the complex, angular momentum of the internal rotor is only loosely coupled to the intermolecular axis. This situation is akin to Hund's 'case d' where the orbital angular momentum of the electron couples weakly to the internuclear axis, but strongly to the rotational angular momentum [30]. Small interaction potential energies are said to be related to slow precession of the internal rotor angular momentum vector ($\vec{j}$) about the intermolecular axis [17]. So for a given precession period, there are many rotations of the complex and the internal angular momentum vector can be considered static. This is referred to by Hutson [29] as *couping case 1*. It essentially means that a quantum number associated with the rotation of the internal rotor is still good—that is, the internal rotor can be considered *decoupled* from the complex and relatively unhindered in its rotation. In reality, the coupling is not completely absent if there is a bound van der Waals state and so perturbation theory can be used to adjust the energy levels.

Table 1.1: Coupling regimes for pseudo-diatomic molecules. V, here, is the anisotropy of the potential

Coupling	Scheme	Description
case 1	V $\ll B \ll b$	free rotor regime
case 2	B $\ll V \ll b$	semi-rigid rotor
case 3	B $\ll b \ll V$	rigid-rotor

The opposite of the 'free' rotor regime of the pseudo-diatomic coupling case 1 is a situation similar to Hund's 'case a'. The coupling energy of the internal to external angular

---

[12] where $\vec{\ell}$ is represents rotation of the complex; that of the internal rotor. Both vectors couple to give

momentum vectors of the pseudo-diatom is much greater than *both* the rotational energy of the complex as well as that of the internal rotor. This leads to fast precession of $\vec{j}$ about the intermolecular axis relative to the rotational period of the complex where the coupling of $\vec{j}$ to the intermolecular axis preserves only it's projection onto that axis, $\vec{j_z}$. Here, since $\vec{j_z}$ couples to the rotation of the complex, ℓ is spoiled and both j and ℓ are bad quantum numbers. Such a coupling scheme bears resemblance to the Hund's 'case a' situation where the orbital angular momentum (and, to be complete, the spin) couples strongly to the internuclear axis and the projection, Λ (Ω with spin), then couples to the rotational angular momentum. The pseudo-diatomic analogue of Hund's 'case a' is the referred to as pseudo-diatomic *coupling case 3*. Suppose now that the interaction potential of the pseudo-diatom is greater than the rotational energy of the complex, but *not* greater than the rotational energy of the internal rotor. In this potential energy regime, the angular momentum of the internal rotor is only moderately coupled to the intermolecular axis. The projection of $\vec{j}$ remains conserved while j is only 'nearly-good' and ℓ is again spoiled by the coupling.[13] This is considered an intermediate example of Hund's 'case a' and is referred to as pseudo-diatomic *coupling case 2*. Efficiency in the Hamiltonian can be had by using a rotated reference frame where the figure axis coincides with the pseudo-diatomic axis. This is done, as presented previously, by passively transforming the space-fixed coordinate frame to a *body-fixed* representation via the appropriate Euler rotation.[14].

Determining the energy levels of the pseudo-diatom can proceed straightforwardly. Contributions to the total internal energy of RG-diatom system comes from the rotation of the entire complex, the internal energy of a diatomic molecule, and the potential that binds the monomers. By considering the pseudo-diatom rigid, R is fixed and the body-fixed Hamilto-

---

[13] Since ℓ is no longer well-defined, the vector ($\vec{J}$-$\vec{j}$) is the vector suitable for describing the rotation of the complex. This vector is appropriate because the total angular momentum vector, $\vec{J}$, is still a well-defined

[14] all functions and operators are adjusted accordingly (not shown here) by using the *xyz* argument that relates to *XYZ* by the direction cosines

nian of equation 1.27 can be simplified.

$$H = \frac{\hbar^2}{2\mu}\left(-\frac{\partial^2}{\partial R^2} + \frac{(\mathbf{J}-\mathbf{j})^2}{R^2}\right) + V(R,\theta) + \mathbf{H}_{mon} \tag{1.27}$$

$$H = \frac{\hbar^2 \boldsymbol{\ell}^2}{2\mu R^2} + V(R,\theta) + b_0\mathbf{j}^2 \tag{1.28}$$

$$H = B\boldsymbol{\ell}^2 + V(R,\theta) + b_0\mathbf{j}^2 \tag{1.29}$$

The lowercase $\mathbf{j}$ is the total angular momentum operator for the monomer and $\boldsymbol{\ell}$ is that for the angular momentum of the entire complex. In the absence of the potential term, the Hamiltonian is just the sum of the pseudo-diatomic Hamiltonian and that for the monomer. Though the electronic potential remains unchanged upon isotopic substitution (i.e. the contour of the surface), this is not true of the expansion representation of the PES [29]. Isotopic substituion displaces the center of mass and so changes the length of R.

1.5 The importance of weakly bound complexes

It is the study of real gases and their deviation from ideal behavior that highlights the importance of the weak bond. Unlike the strong chemical bond (covalent or ionic), governed primarily by the coulomb and exchange interactions between close nuclei [21], energetic contributions to the weak bond are primarily the electrostatic interaction, the induction energy, and the dispersion energy and manifest at long range. The electrostatic interaction is that between separated charge distributions of the weakly bound molecules and is referred to as a dipole-dipole interaction. The induction energy arises from an induced dipole-dipole interaction where the dipole of one species induces a dipole in another. The dispersion energy has no classical analogue and is found between species where correlation of quantum fluctuations in charge distribution causes an induced-dipole induced-dipole interaction [32]. There are many sources [32–34] that discuss the analytical forms of these forces that contribute to the weak bond. Here, those will be collectively referred to as van der Waals forces after the 19th century physicist of the same name who championed the notion that molecules (and atoms) are not infinitely compressible nor do they occupy the maximal, ideal volume. While it is the finite size of molecules that limit the compressibility of a substance, it is the van der Waals forces that are responsible for the different phases of matter [35] and govern properties such as boiling point, vapor pressure, and surface tension.

Weakly bound complexes have special relevance to atmospheric chemistry. With sufficient number densities and low enough temperatures, weakly bound complexes may prove a significant reservoir for reactive species in the atmosphere. The strength of weak bonds typically ranges from 100 to 1000 cm^{-1} [32, 34]. Temperature in the troposphere decreases linearly with increasing altitude (as per the $\sim$10 K/km dry adiabatic lapse rate [36]). Low temperatures ($\sim$215 K at the top of the troposphere—150 cm^{-1}) mean that available thermal energies are not greater than the dissociation energies of many complexes possibly present. Accurately estimating the concentrations of weakly bound complexes can give insight into the impact these species have on the radiative capacity of the atmosphere. Recent work [37, 38] has provided a basis for estimations of weakly bound complex atmospheric abundance to shed light on the potential for these complexes to affect the availability of key atmospheric reactants. The equilibrium structure defined by the complex also affects the photodissociation cross sections of each monomer involved. Because absorbed radiation has to overcome the intermolecular modes, non-radiative outcomes are less likely and photodissociation reaction efficiency along a specified path improves [39, 40].

Chapter 2

Experimental

2.1 Overview

The UGA HENDI instrument is modular in its construction not unlike conventional molecular beam experiments. It consists of four main, in-line aluminum chambers that respectively allow for the generation of the droplet beam, the skimming and collimation of that beam, the doping of droplets, and the mass spectrometric detection of frequencies absorbed by those dopants. Before any spectroscopy commences, the droplet beam must first be generated. This is done by the cold head. The cold head is a conduit that cools and ushers the high-pressure, ultra-pure (99.999995%) ^{4}He to the to its point of effusion into the vacuum system.

2.2 Droplet formation

The formation of superfluid ^{4}He nanodroplets is a process born from collisional cooling. The temperature of the ultrapure ^{4}He must first be dramatically reduced from room temperature. Such a drop in temperature is facilitated by the cooling of a three-stage cold head. The cold head is refrigerated by a closed-cycle helium compressor unit. The ultrapure ^{4}He is piped into the instrument through the cold head via 1/16" copper tubing wound around the first and second stages. The first stage of the cold head is capable of cooling the ^{4}He to 50 K; the second stage as low as 4 K. Attached to the final stage is the nozzle. The third stage is decoupled from the cold head monolith by a Swagelok fitting and is translation-stage mounted for optimal control of the nozzle-skimmer alignment. A Kaptan heater, controlled by PID feedback, allows for sufficiently precise nozzle temperature control. Typical operating conditions for the beam expansion are ∼25 bar and a nozzle temperature between 14–20 K. Supersonic ^{4}He expansion in this regime reliably creates a beam of superfluid nanodroplets. It was determined from mass spectrometric cross-beam scattering experiments [41] that the radial distribution of a scattered helium beam maps neatly onto a log-normal droplet size distribution. Such a distribution suggests that the variance in the most probable droplet size scales linearly as the natural log of that droplet size.

2.3 Droplet doping

Before spectroscopy is done, droplets must first be doped. To optimize spectroscopy signal from a single species, it is necessary to consider the likelihood that one droplet will capture one dopant. It is assumed that a doping event is independent of all other doping events. Each droplet that passes the doping region without being doped is categorized as a failure and one that is—a success. The doping region has some fixed dimension and the droplets are taken as having constant size and distance between droplets. It is also assumed that potential dopants have a random probability of doping a droplet while in the doping region. Such a construct is basically a Bernoulli trial [42]. When N total number of droplets exit the doping region, k number of droplets will have been successfully doped while N-k number of droplets will be empty. The probability of a single dopant doping a single droplet is denoted as p and the probability of not doping is q. The likelihood of obtaining the given sequence of N droplets exiting the doping region, B_k, is the product of independent event probabilities associated with each droplet

$$B_k(n,p) = ppqqqpq \cdots = p^k q^{n-k}, \tag{2.1}$$

where the exponents in the product are the number of doped (k) and empty (n-k) droplets in the sequence. The order of the droplets is irrelevant. This gives N! number of ways to organize them. For a given sequence though, there is redundancy in the number of ways to configure the sequence. Permutations of only the doped droplets or only the empty ones yield an equivalent configuration. The likelihood of receiving a given number of doped and empty droplets is weighted by the number of ways the sequence can be uniquely written. This is the binomial distribution where the number of dopants, n, chooses k number of droplets.

$$B_k(n,p) = \binom{n}{k} p^k q^{n-k} = \frac{n!}{k!(n-k)!} p^k q^{n-k} \tag{2.2}$$

This is the Binomial distribution. In the actual HENDI experiment, the number of droplets and dopants is very large. This means that p→0 and so does the Binomial distribution in the limit of many droplets. Such a result is confounding because regardless of how disparate the dopant-to-droplet ratio becomes, doping is still happens. The more appropriate question to ask is of the *the average number of dopants per droplet* that is most likely under given expansion conditions. The average number of dopants per droplet, μ, is defined as follows

$$\mu = pn = \frac{n}{N} = \frac{\text{number of dopants}}{\text{number of droplets}} \tag{2.3}$$

$$\text{where } p = \frac{1}{N}, \tag{2.4}$$

and the number of dopants can be written as μN. Returning to the expression for the binomial distribution of equation 2.2, it can now be written in terms of μ. Rearrangement of the binomial distribution can be shown to have an convenient form in the limit of large n and is featured below

$$B_k(\mu N, p) = \binom{\mu N}{k} p^k q^{n-k} = \binom{\mu N}{k} \frac{1}{N}^k \left(1 - \frac{1}{N}\right)^{n-k} \tag{2.5}$$

$$= \frac{n(n-1)(n-2)\cdots(n-k+1)}{k!} \frac{\mu}{n}^k \left(1 - \frac{\mu}{n}\right)^n \left(1 - \frac{\mu}{n}\right)^{-k} \tag{2.6}$$

$$= \frac{n(n-1)(n-2)\cdots(n-k+1)}{n^k} \frac{\mu}{k!}^k \left(1 - \frac{\mu}{n}\right)^n \left(1 - \frac{\mu}{n}\right)^{-k} \tag{2.7}$$

$$= \frac{\mu}{k!}^k \left(1 - \frac{\mu}{n}\right)^n \left[\left(1 - \frac{1}{n}\right)\left(1 - \frac{2}{n}\right)\cdots\left(1 - \frac{k+1}{n}\right)\left(1 - \frac{\mu}{n}\right)^{-k}\right] \tag{2.8}$$

$$\lim_{n\to\infty} B_k = \frac{\mu}{k!}^k e^{-\mu} \tag{2.9}$$

This is the Poisson distribution. Similar expressions have been derived empirically [43, 44].

The likelihood of doping a droplet of a given average size is then the joint probability of obtaining a droplet of some average size and doping it with an average number of dopants. It is the product of likelihoods regarding these two conditions that govern what can be called the droplet occupation probability.

Dopants are introduced perpendicular to the beam path. This is done by way of a load-lockable port or static gas manifold. The pyrolysis source is introduced through the load-loackable port to avoid the need to vent the vacuum system whenever a new precursor is to be pyrolyzed. The source itself is a KF40 flange tapped by four, tubular electrical feedthroughs with a single cajon fitting situated in the middle of the feedthroughs coupled to a Swagelok fitting through the flange. Each couple of tubular feedthroughs has a copper tube loop welded to it. The cajon fitting serves to situate the quartz pyrolysis tube that traverses the length of the source and is the conduit through which precursor gas is flowed.

A space-separated, copper head unit clamps together the bend of each copper tube loop and also allows for the passage of the quartz tube. The quartz tube protrudes past the face of the copper head unit by 1" and is straddled by a pair of threaded brass (or copper) rods that are received by the copper head unit. Tantalum wire is wrapped around the quartz tube and secured to the protruding threaded rods. The copper tube loops encased in the copper head unit serve a dual purpose: to deliver current to the tantalum wire and to allow for water cooling. Current to the tantulum wire heats the filament resistively that, in turn, radiatively heats a quartz tube. This creates a hot zone that pyrolyzes the flowed precursor. The pyrolysis source can be laterally situated such that pyrolysis products are introduced directly into the droplet beam. Downstream from the pyrolysis source is situated a cylindrical tube spanning the perpendicular width of the chamber. This cylindrical tube, referred to as the pick-up cell (PUC), is evacuated by a separate diffusion pump and is fed by a Swagelok gas manifold capable of co-mingling two separate dopant gases.

Upon doping a droplet, thermal energy of the dopant is rapidly quenched [45] (on the nanosecond time-scale; $\sim 10^6$ times shorter than the droplet time-of-flight through the instrument) by the transfer of energy mostly to the translational modes of helium atoms via evaporation. Such evaporation dissipates ~ 5 cm^{-1} of thermal energy per atom. Attainment of thermal equilibrium via helium evaporation leaves the doped droplet with a smaller ionization cross-section than empty droplets. The cross-section of the droplet beam can then be seen as dependent on the amount of energy absorbed by the dopant degrees of freedom and subsequently transferred to the droplet.[1]

---

[1] this phenomenon is interesting in its own right as some systems exhibit anomalous line inhomogeneities which have been interpreted [46] as energetic coupling to quantum modes of the bulk droplet

2.4 The laser system

Resonances of dopants trapped in the superfluid helium nanodroplets are induced using the Acculight Argos 2400 laser system. This system generates continuous wave radiation through the region of 2550–4000 cm^{-1}. Light is initiated in a fiber seed laser and amplified to 15 W by a master oscillator power amplifier. The amplified light constitutes the *pump beam* that is collimated and directed towards the optical parametric oscillator. The OPO is a monolithic bowtie cavity with a birefringent, periodically poled LiNbO$_3$ crystal as the quasi-phase-matching gain medium. The pump beam generates the *signal* beam which is at lower frequency since it is in resonance with the cavity. Both the pump and the signal beam exit the cavity after one pass. The *idler* beam is the difference between the pump and the signal beam frequency as shown below.

$$\frac{1}{\lambda_{idler}} = \frac{1}{\lambda_{pump}} + \frac{1}{\lambda_{signal}} \tag{2.10}$$

It is the idler beam that gives light within the aforementioned infrared region. With the frequency of the pump beam fixed, controlling the signal beam frequency allows for smooth tuning of the idler beam [47]. This is done be adjusting the angle of incidence the pump beam has with the gain crystal. Idler output power from the OPO is typically 2 W.

Phase-modulated laser radiation is guided into the instrument counter-propagating along the beam path. It is the frequency-dependent decrease in cross-section that serves as the spectroscopic signal. Droplets enter an electron impact ionization region (typically ∼90 eV) and the charge of an ionized helium atom quickly diffuses [48] throughout the droplet and towards the dopant. This charge diffusion process is spontaneous and fast because of the large ionization energy of ^{4}He (24.6 eV) relative to the dopants (∼7-11 eV). A quadrupole mass spectrometer serves as a mass filter and is tuned to detect fragments associated with the dopant. Once a mass channel attributable to the dopant of interest is identified, ion signal on that mass channel is monitored as laser frequency is scanned. Resonances are detected as ion signal depletion. Since the laser light is square-wave modulated (by a chopper), ion depletion signal can be continuously compared to ion signal generated from non-irradiated droplets. It is from this comparison that the spectrum is derived.

Chapter 3

Results

3.1 The spectrum of the OH-CH_4 complex

The OH-CH_4 complex has been captured in ^{4}He nanodroplets and its infrared spectrum collected in the region of hydroxyl radical absorption centered 3562.08 cm^{-1}. This position constitutes an approximate 3 cm^{-1} shift from the free OH in ^{4}He. This shift makes sense especially in light of the work by Lester et al on the same system [3]. They report a shorter vibrational lifetime for the OH radical in the complex upon overtone excitation. This implies an efficient relaxation mechanism of vibrational energy from the OH to CH_4. Such a process would require significant coupling between the monomers. This effect can slightly reduce the bond strength [49]. A series of spectra of the OH-CH_4 isotopologues are collected. The first is the OD-CH_4, then the OH-CD_4, and finally the OD-CD_4 spectrum. The overlaid spectra are shown in figure 3.1 and what can be seen from this systematic isotopic substitution is the disappearance of the splittings so apparent in the OH-CH_4 spectrum. In the OD-CD_4, the splittings are not resolved. It is thought that by weighting the molecule and changing the rotational energy, the ability of the anisotropic potential to couple angular momenta is affected.

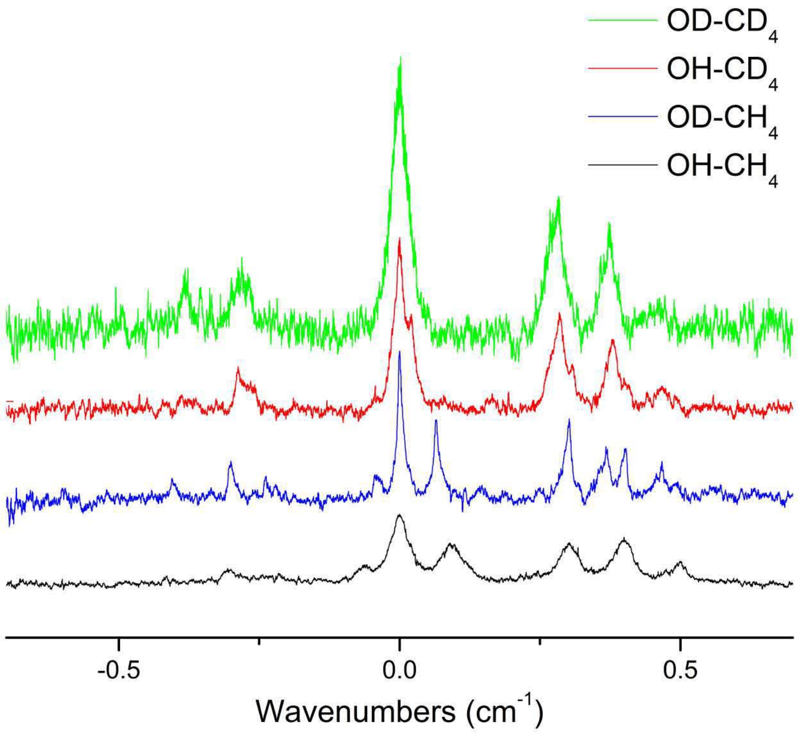

Figure 3.1: Rovibration spectra of $OH\cdots CH_4$ and its deuterated isotopologues

Exchanging OD for OH in the initial complex should serve to reduce the effective rotational constant of the complex. This serves to increase the rotational state density. The splitting still present in the OD complex suggests that the strength of the anisotropy is still intermediate relative to the rotational constants and only hinders internal rotation. The OD complex is in a case 2 situation (as mentioned in section 1.3). Deuteration of the methane rather than the OH reduces the rotational constant of the complex considerably. At this point the splittings are very small which suggests that the rotational energy of the complex on on the order of the interaction energy. The final isotopologue completes the adjustment of the rotational energy by definitively reducing it below the energy of interaction. The complex now has bound states as the interaction energy has overtaken internal rotation. As evidenced from the symmetric top-like spectrum, the complex should now behave like a rigid molecule.

3.2 The Hamiltonian and the PES

The Hamiltonian used is the typical pseudo-diatomic Hamiltonian presented in section 1.3. Rotational constants for methane and the complex are taken from [50]. The matrix elements of the Hamiltonian are given by Ohshima and Endo [51]. In their evaluation, the "helicity decoupling approximation" is ignored and the off-diagonal elements of the ℓ^2 operator are included.[1] In accordance with Oshima and Endo, the spherical tensor approximation for the potential is used and successfully reproduces the general trends in their correlation diagram. This is not surprising since their representation of the potential

$$T^{(3)} = C_{3,-2}(\theta, \chi) - C_{3,2}(\theta, \chi) \tag{3.1}$$

transforms precisely as the tetrahedron—as methane. Below is a diagram of how select states evolve with increasing anisotropy. Neglecting helicity decoupling introduces splittings that have yet to be quantified in this model.

---

[1] although their inclusion did not significantly affect the correlation diagram

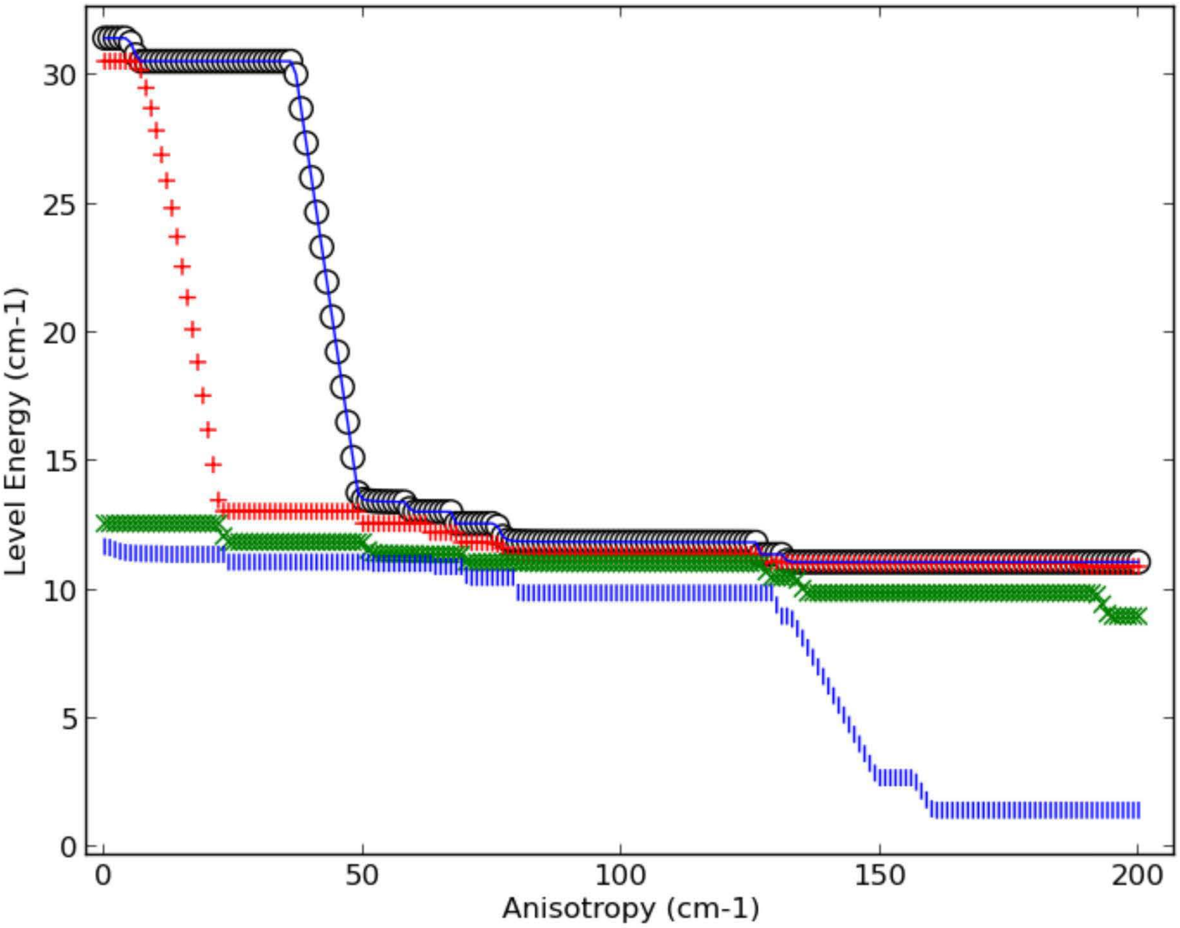

Figure 3.2: Progression of states as a function of anisotropy

Chapter 4

Conclusion and Outlook

What has been presented here is only part of the solution. It would be appropriate to quantify the difference between the different approaches (helicity decoupling approximation, spherical tensor contraction, etc.) to generating the correlation diagram between the free internal rotor and rigid rotor situations. Also, explicit inclusion of half integer spin in the Hamiltonian. Of vital importance though is the simulation of the spectrum. In preliminary tests, code written to extract eigenvalues from diagonalized Hamiltonians for plotting was also used to display the free rotor states that mix in order to compose the wavefunctions of the rigid system. State labeling is still an issue. The reported pattern of degeneracy [51] has yet to be repeated. This system is a prototype for more complicated polyatom-polyatom systems whose spectra await analysis ($O_3 \cdots H_2O$ and $O_3 \cdots C_2H_4$). Unlike in the $OH \cdots CH_4$, these more complicated systems have monomers each with three rotational degrees of freedom. Considering such systems will definitely require a more sophisticated angular momentum coupling scheme.

Bibliography

[1] Kirschke, S.; et al. *Nat. Geosci.* **2013**, *6*, 813–823.

[2] Atkinson, R. *Atmos. Chem. Phys. Discuss.* **2003**, *3*, 4183–4358.

[3] Wheeler, M. D.; Anderson, D. T.; Lester, M. I. *Int. Rev. Phys. Chem.* **2000**, *19*, 501–529.

[4] Steinfeld, J. I.; Francisco, J. S.; Hase, W. L. *Chemical Kinetics and Dynamics*, 2nd ed.; Prentice-Hall Inc.: Upper Saddle River, NJ, 1998.

[5] Shannon, R. J.; Blitz, M. a.; Goddard, A.; Heard, D. E. *Nat. Chem.* **2013**, *5*, 745–9.

[6] Donahue, N. M. *Chem. Rev.* **2003**, *103*, 4593–604.

[7] Griffiths, D. J. *Quantum Mechanics*, 1st ed.; Prentice Hall, Inc.: Upper Saddle River, NJ, 1995.

[8] Johnson, Jr., C. S.; Pendersen, L. G. *Problems and Solutions in Quantum Chemistry and Physics*, 1st ed.; Dover Publications: New York, NY, 1986.

[9] Bernath, P. F. *Spectra of Atoms and Molecules*, 1st ed.; Oxford University Press: New York, NY, 1995.

[10] Harris, D. C.; Bertolucci, M. C. *Symmetry and Spectroscopy*; Dover Publications: New York, NY, 1978.

[11] Nesbitt, D. J.; Suhm, M. a. *Phys. Chem. Chem. Phys.* **2010**, *12*, 8151.

[12] Bunker, P. R.; Jensen, P. *Molecular Symmetry and Spectroscopy*, 2nd ed.; NRC Research Press: Ottawa, 2006.

[13] Bunker, P. R.; Jensen, P. *Fundamentals of Molecular Symmetry*; IOP Publishing: London, 2005.

[14] Slipchenko, M. N.; Sartakov, B. G.; Vilesov, A. F.; Xantheas, S. S. **2007**, *111*, 7460–7471.

[15] Dong, F.; Roberts, M.; Nesbitt, D. J. *J. Chem. Phys.* **2008**, *128*, 044305.

[16] Raston, P. L.; Liang, T.; Douberly, G. E. *J. Chem. Phys.* **2013**, *138*, 174302.

[17] Bratoz, S.; Martin, M. L. *J. Chem. Phys.* **1965**, *42*, 1051.

[18] Dunker, A. M. *J. Chem. Phys.* **1976**, *64*, 354.

[19] Holmgren, S. L.; Waldman, M.; Klemperer, W. *J. Chem. Phys.* **1977**, *67*, 4414.

[20] Weida, M. J.; Sperhac, J. M.; Nesbitt, D. J.; Hutson, J. M. *J. Chem. Phys.* **1994**, *101*, 8351.

[21] Levine, I. *Quantum Chemistry*, 6th ed.; Pearson Prentice Hall: Upper Saddle River, NJ, 2008.

[22] Edmonds, A. R. *Angular Momentum in Quantum Mechanics*; Princeton University Press: Princeton, NJ, 1957.

[23] Brink, D.; Satchler, G. R. *Angular Momentum*, 3rd ed.; Clarendon Press: Oxford, 1993.

[24] Zare, R. N. *Angular Momentum*; John Wiley & Sons: Canada, 1988.

[25] Wolf, A. A. *Am. J. Phys.* **1969**, *37*, 531.

[26] Harter, W. G. *Principles of Symmetry, Dynamics, and Spectroscopy*; John Wiley & Sons, Inc., 1993.

[27] Morrison, M. A.; Parker, G. A. *Aust. J. Phys.* **1987**, *40*, 465.

[28] Balle, T. J.; Campbell, E. J.; Keenan, M. R.; Flygare, W. H. *J. Chem. Phys.* **1980**, *72*, 922.

[29] Hutson, J. M. In *Adv. Mol. Vib. Collis. Dyn.*, 1st ed.; Bowman, J. M.; Ratner, M. A., Eds.; JAI Press, Inc., 1991; Vol. 1, pp 1–46.

[30] Herzberg, G. *Molecular Structure and Spectra: I. Spectra of Diatomic Molecules*, 2nd ed.; D. Van Nostrand Company, Inc.: Princeton, NJ, 1950.

[31] Nikitin, E. E.; Zare, R. N. *Mol. Phys.* **1994**, *82*, 85–100.

[32] Havenith, M. *Infrared Spectroscopy of Molecular Clusters*; Berlin, Germany: Berlin, Germany, 2001.

[33] Duxbury, G. *Infrared Vibration-Rotation Spectroscopy*; John Wiley & Sons Ltd.: West Sussex, England, 2000.

[34] Stone, A. *The Theory of Intermolecular Forces*; Oxford University Press: New York, 1996.

[35] McQuarrie, D. A. *Statistical Mechanics*, 1st ed.; Viva Books Private Limited: Vivad, Vasishtha, 2003.

[36] Hartmann, D. *Global Physical Climatology*; Acadmic Press: San Diego, CA, 1994.

[37] Vaida, V.; Headrick, J. E. *J. Phys. Chem. A* **2000**, *104*, 5401–5412.

[38] Murray, C.; Derro, E. L.; Sechler, T. D.; Lester, M. I. *Acc. Chem. Res.* **2009**, *42*, 419–27.

[39] Klemperer, W.; Vaida, V. *Proc. Natl. Acad. Sci. U. S. A.* **2006**, *103*, 10584–8.

[40] Schinke, R. *Photodissociation Dynamics*; Oxford University Press: Oakleigh, Victoria, 1993.

[41] Lewerenz, M.; Schilling, B.; Toennies, J. *Chem. Phys. Lett.* **1993**, *206*, 381–387.

[42] Haken, H. *Synergetics*, 2nd ed.; Springer-Verlag: Berlin, Germany, 1978.

[43] Lewerenz, M.; Schilling, B.; Toennies, J. P. *J. Chem. Phys.* **1995**, *102*, 8191.

[44] Lugovoj, E.; Toennies, J. P.; Vilesov, A. *J. Chem. Phys.* **2000**, *112*, 8217–8220.

[45] Brink, D.; Stringari, S. *Zietschrift für Physiakalische Chemie* **1990**, *15*, 257–263.

[46] Morrison, A. M.; Raston, P. L.; Douberly, G. E. *J. Phys. Chem. A* **2013**, *117*, 11640–7.

[47] Demtröder, W. *Laser Spectroscopy*, 2nd ed.; Springer-Verlag: Berlin, Germany, 1995.

[48] Ellis, A.; Yang, S. *Phys. Rev. A* **2007**, *76*, 032714.

[49] Joseph, J.; Jemmis, E. D. *J. Am. Chem. Soc.* **2007**, *129*, 4620–32.

[50] Wheeler, M. D.; Tsiouris, M.; Lester, M. I.; Lendvay, G. *J. Chem. Phys.* **2000**, *112*, 6590.

[51] Ohshima, Y.; Endo, Y. *J. Chem. Phys.* **1990**, *93*, 6256.